Linear, two- and four-armed pyridine-decorated thiazolo[5,4-d]thiazole fluorophores: Synthesis, photophysical study and computational investigation

Abdelaziz Jouaiti, Valerio Giuso, Cristina Cebrián, Pierluigi Mercandelli, Matteo Mauro

Linear, two- and four-armed pyridine-decorated thiazolo[5,4-*d*]thiazole fluorophores: synthesis, photophysical study and computational investigation

Abdelaziz Jouaiti,[a,] Valerio Giuso,[b] Cristina Cebrián,[c] Pierluigi Mercandelli,[d] Matteo Mauro[b,]**

[a] Laboratoire de Synthèse et Fonctions des Architectures Moléculaires, UMR7140 Chimie de la Matiere Complexe, Institut Le Bel, Université de Strasbourg & CNRS, 4 rue Blaise, Pascal 67000 Strasbourg (France), e-mail : jouaiti@unistra.fr

[b] Institut de Physique et Chimie des Matériaux de Strasbourg, UMR7504, Université de Strasbourg & CNRS, 23 rue du Loess, 67000 Strasbourg, France, e-mail : mauro@unistra.fr

[c] Laboratoire Lorraine de Chimie Moléculaire (L2CM), Université de Lorraine, CNRS, F-57000 Metz, France

[d] Dipartimento di Chimica, Università degli Studi di Milano, via Camillo Golgi 19, 20133 Milano, Italy

Highlights

- Nine novel thiazolo[5,4-*d*]thiazole fluorophores with peripheral pyridines is presented.
- The compounds possess either a linear, two- or four-armed molecular structure.
- All the compounds display good near-UV to bluish-green fluorescence.
- Linear derivatives show better photoluminescence quantum yields compared to non-linear counterparts up to 0.42.
- The nature of the short-lived excited state is confidentially described as π-π*.

Abstract

A novel family of thiazolo[5,4-*d*]thiazole (TzTz) fluorophores having a general formula (**py**)$_n$-**π-TzTz-π-**(**py**)$_n$ (*n* = 1 or 2, py = pyridine) is herein reported. The investigated compounds are decorated with alkoxy-substituted pyridine scaffolds bearing chains with different lengths (**a** = methoxy, **b** = 2-ethylhexan-1-oxy, **c** = 2-decyltetradecan-1-oxy) that are connected at either the *para*- or *meta*- position(s) of the phenyl bridging ring. The compounds feature either a linear (*n* = 1, *para*-substituted, series **8**), two-armed (*n* = 1, *meta*-substituted series **9**) or four-armed (*n* = 2, *meta*-substituted series **10**) molecular architecture. Steady-state and time-resolved photophysical investigation is employed to characterize the optical properties of the compounds in both diluted CH_2Cl_2 and CH_2Cl_2:trifluoroacetic acid (TFA) 95:5 solutions, as well as in thin-film in *poly*(methyl methacrylate) (PMMA) matrix at 20 wt.% doping. All compounds display electronic transitions with mainly π-π* nature at both solution and solid state. However, while both peripheral pyridyl-phenyl moieties and the π-**TzTz**-π core participate in the absorption transitions, the emission involves mostly the π-**TzTz**-π core. A clear effect of the positional isomerism on the photophysical properties is observed, with the protonation of the peripheral pyridines offering a further modulation. Thus, these results provide some useful hints on the molecular design of TzTz-based compounds as promising photoactive materials.

Graphical abstract

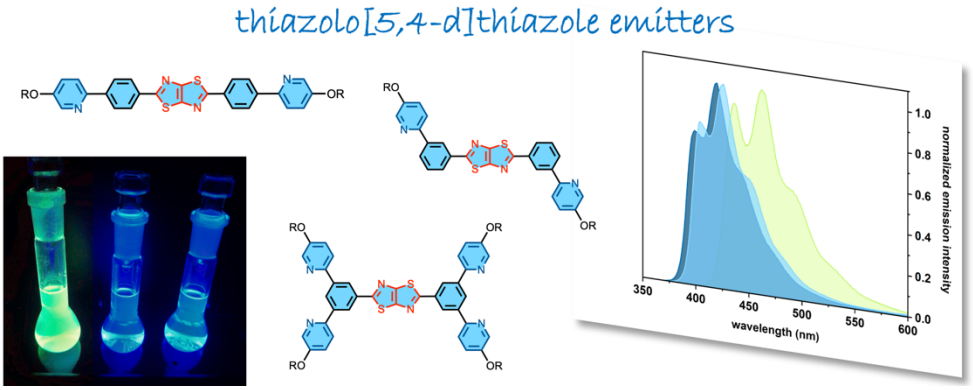

A novel family of near-UV to bluish-green emitting thiazolo[5,4-*d*]thiazole chromophores is presented and their optical properties investigated by jointly photophysical and computational techniques.

Keywords

thiazolo[5,4-d]thiazole; fluorescence; organic emitters; N-heterocycles; mixed heterocycles; density functional theory

Introduction

Small-molecule organic dyes have attracted enormous interest in both materials and biological sciences driven by their potential and real-market application in several fields. In particular, they found widespread use as emitting, lasing and semiconducting materials in optoelectronic devices,[1-3] such as organic light emitting diodes (OLEDs) and light-emitting field-effect transistors (OLEFET), as well as light-harvesting devices[4]. Heterocyclic compounds that contain one or more endocyclic nitrogen atoms are amongst the most investigated classes of small-molecule emitters, including (substituted) carbazoles, (benzo)diazoles, (benzo)triazoles, and triazines.[5] Sulfur-containing (fused) heterocycles, typically incorporating (benzo)thiazole and (benzo)thiophene scaffolds, have been largely investigated as well, mainly for their excellent charge transport and light-absorption properties that render these chromophores appealing molecular materials for organic electronics,[6-7] organic photovoltaics,[8] and non-linear optics.[9]

Small-molecule containing mixed heterocyclic scaffolds represent another family of compounds with very appealing optical properties.[10] The thiazolo[5,4-*d*]thiazole (**TzTz**) scaffold is a bicyclic heteroaromatic system formally obtained by the fusion of two thiazole rings. TzTz and its derivatives feature an electron-deficient aromatic moiety that favours rather coplanar conformations in polycyclic systems due to the absence of interactions between ortho H atoms, thus enabling intermolecular interactions. Owing to the ease of their synthesis, which typically is carried out via a double condensation reaction between dithiooxamide and an aromatic aldehyde under oxidative conditions,[11,12] and their appealing electronic properties,[11,13,14] TzTz-based molecular materials with either symmetric or asymmetric architectures have recently started to gain attention in the field of small molecule materials for organic electronics,[15-20] as well as bioimaging[21] and chemo-sensing probes[22-23]. In particular, neutral 2,5-*bis*(hetero)aryl functionalized TzTz derivatives possess short-lived (a

few ns) and PLQY in the range of *ca.* 0.2.[24] Interestingly, protonation or alkylation of the peripheral N-containing heteroaromatic rings (generally pyridine, py), may enhance the emission efficiency of the TzTz-based emitters, which in some cases approaches unity.[25] These cationic derivatives have shown to possess an interesting combination of outstanding redox and optical properties,[26,27] and demonstrated to be suitable candidates as NIR dyes,[28] and highly fluorescent electrofluorochromic materials[25]. Surprisingly, limited attention has been paid to the effect of structural variation and isomerism in this class of excellent fluorophores, being 2,5-*bis*(pyridyl)-TzTz and their N-alkylated derivatives the most investigated ones to date. It is indeed worth to notice that organic semiconducting molecules with peripheral pyridines are known to possess enhanced charge transport properties.[29-31] In view of their excellent optical and electronic features as well as straightforward synthetic accessibility, we aim at investigating the effect of the number of pyridyl moieties and the corresponding positional isomerism onto their photophysical properties. Herein, the synthesis, steady-state and time-resolved photophysical investigation of a novel set of free-base and protonated peripheral pyridine-decorated TzTz fluorophores is described. Optical properties were further elucidated by means of a computational study at (time-dependent) density functional theory, namely (TD-)DFT, level. In particular, we report on deep blue to bluish-green emitting TzTz chromophores with general formula (**py**)$_n$-**π**-**TzTz**-**π**-(**py**)$_n$ (n = 1 or 2) with either a linear (series **8**), two-armed (series **9**) or four-armed (series **10**) molecular architecture before and after protonation.

Results and Discussion

Synthesis

In Scheme 1 are displayed the final steps for achieving the novel fluorophores (**8**–**10**) featuring the thiazolo[5,4-*d*]thiazole core, with the full synthetic details being described in the Supporting

Information. All the intermediates and final compounds were characterized by ^{1}H, ^{13}C NMR as well as mass-spectrometry analysis (see Figure S1–S26 of the Supporting Information), except for derivative **8a** that displayed limited solubility in many different organic solvents, thus hampering its complete characterization.

While pyridine derivative **1a** is commercially available, **1b** and **1c** were prepared in good to excellent yields upon alkylation of 2-bromo-5-hydroxypyridine by using either 2-ethylhexyl bromide or 2-decyltetradecyl tosylate, respectively, in hot DMF and K_2CO_3 as the base. On the other hand, the brominated **TzTz** derivatives (**2**–**4**, see Supporting Information for chemical structures) were synthetized straightforwardly by condensation reaction between the dithiooxamide and the corresponding bromobenzaldehyde following the procedure reported previously for related TzTz derivatives.[11,12]

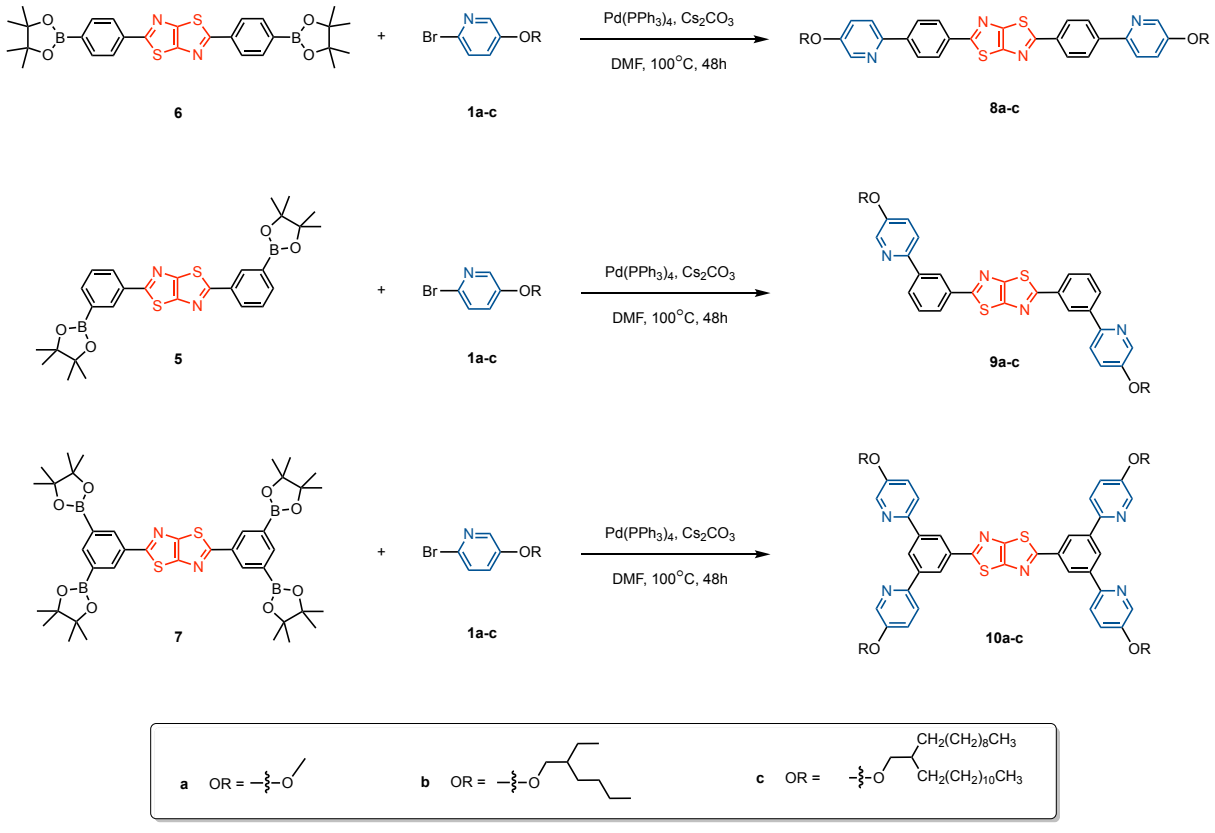

Scheme 1. Schematic pathway for the synthesis of luminophores **8**–**10**.

Subsequently, cross-coupling reaction between aryl-bromine **2**–**4** and bis(pinacolato)diboron under palladium-catalyzed Miyaura borylation conditions afforded either *bis*- (**5**–**6**) and *tetra*- (**7**) pinacoleboronate derivatives with excellent yields. Finally, Suzuki-Miyaura cross-coupling between the boronate **5**–**7** and 2-bromo-5-alkoxypyridine (**1a**–**c**) enables the introduction of peripheral pyridine rings, thus providing the target novel TzTz compounds of general formula (**py**)$_n$-**π**-**TzTz**-**π**-(**py**)$_n$. Overall, the compounds display molecular structures with either a linear (*n* = 1, *para*-substituted, series **8**), two-armed (*n* = 1, *meta*-substituted series **9**) or four-armed (*n* = 2, *meta*-substituted series **10**) architecture (see Scheme 1).

Optical properties

Firstly, the photophysical properties of derivatives **8**–**10** were investigated by means of steady-state and time-resolved photophysical techniques in air-equilibrated solution CH_2Cl_2 at room-temperature The electronic UV-Vis absorption and photoluminescence spectra in solution are displayed in Figure 1, respectively, for compound **8b**–**10b.** The absorption and emission spectra of all the compounds can be found in Figure S27–S28 (see Supporting Information), respectively, for comparison and the corresponding photophysical data and fluorescence kinetics parameters are summarized in Table 1.

Among the compounds under investigation, methylated derivatives (series **a**) display lower solubility. In particular, it was not possible to carry out proper photophysical characterization of compound **8a**. Therefore, longer alkyl chains (series **b** and **c**) were introduced to improve the solubility, thus ruling out possible ground state intermolecular interactions in solution through π-stacking, which would be favored by the extended π-conjugated nature of the chromophores. As shown in Figure S27 of the Supporting Information, the photophysical properties appear to be rather independent of the length of the peripheral

alkyl chain for a given series of compounds. This is attributed to the rather similar electronic properties exerted by the different alkyl substituents onto the heteroaromatic rings between series **a**, **b** and **c**. Hence, only the optical properties of series **b** will be detailed hereafter, with similar conclusions drawn for the other two series. In dilute CH_2Cl_2, samples of compound **8b**-**10b** display two main intense absorption bands in the region at about 360 and 270 nm. As far as the linear compound **8b** is concerned, the absorption band present at longer wavelength is much more intense and bathochromically shifted compared to those recorded for the *meta*-substituted derivatives, being $\lambda_{abs,max}$ = 392 ($\varepsilon \approx 6.7\times10^4$ M^{-1} cm^{-1}), 364 ($\varepsilon \approx 4.2\times10^4$ M^{-1} cm^{-1}) and 367 nm ($\varepsilon \approx 4.7\times10^4$ M^{-1} cm^{-1}), for **8b**, **9b** and **10b**, respectively.

At higher energy in the spectral region above λ_{abs} = 320 nm, the trend appears to be the opposite with the absorption band of compound **8b** being the least intense among the series ($\varepsilon \approx 2.1\times10^4$ M^{-1} cm^{-1} at 267 nm); whereas $\varepsilon \approx 2.9–3.6\times10^4$ M^{-1} cm^{-1} and $6.0–6.2\times10^4$ M^{-1} cm^{-1} for compounds **9b** and **10b**, respectively. On the basis of these spectral findings, one can ascribe both bands, namely the higher and lower energy spectral profiles, with confidence to the convolutions of electronic transitions involving the π-TzTz-π moiety mainly with sizeable singlet-manifold ligand-centered ^{1}LC π-π* with partial admixed intraligand charge-transfer (ICT) character ($\pi_{ROpy}\pi_{TzTz} \rightarrow \pi^*_{phenyl}$). The fact that the intensity of the high energy band doubles on going from compounds **9b** to **10b**, while the lower-energy side appears to be affected to a much lower extent by the number of pyridine substituents, further corroborate these attributions, which are also in agreement with previously reported data for related chromophores,[24,25] as well as with the computation investigation described below. Moreover, the absorption maximum wavelengths are affected to only a little extent by the number of pyridine substituents, with bathochromic shift as small as *ca.* 300 cm^{-1} between series **9** and **10**. In sharp contrast, absorption spectra of compounds of the series **8** appear to be bathochromically shifted by about 2000 cm^{-1}. These findings point toward a reduced π-conjugation and limited

electronic communication between the *meta*-oriented N-heterocyclic rings and the TzTz core in compound **9b**–**10b** with respect to *para*-oriented scaffolds (*i.e.* compound **8b**).

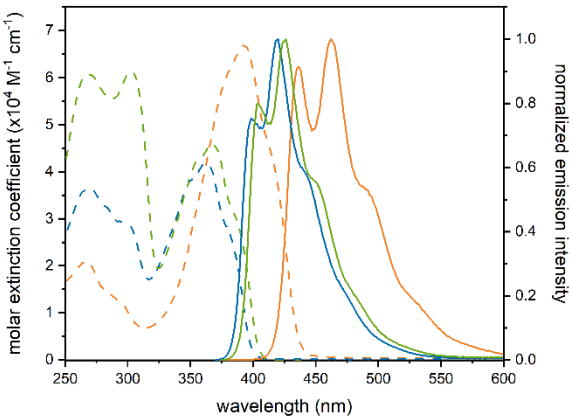

Figure 1. Electronic absorption (dashed traces) and normalized emission (solid traces) spectra of compound **8b** (orange), **9b** (blue), and **10b** (green) in air-equilibrated CH_2Cl_2 at a concentration of 5×10^{-6} M at room temperature. Emission spectra were recorded upon excitation at λ_{exc} = 350 nm.

Upon photoexcitation at λ_{exc} = 300–370 nm, solution samples of all the derivatives in CH_2Cl_2 at concentration as low as 5×10^{-6} M display intense blue luminescence with emission onsets falling in the near-UV region, as shown in Figure 1. As expected, while emission maxima appear to be independent of the nature of the alkyl chain, they are much more influenced by the positional isomerism of the pyridine peripheral substituents. Compound **9b** displays a photoluminescence profile with emission maxima at 399, 419 and 442 nm. *Meta*- disubstituted derivative **10b** shows a rather similar, yet bathochromically shifted, spectrum by about 5 nm (*ca.* 330 cm^{-1}). On the other hand, *para*-substituted compound **8b** possess an emission profile peaking at λ_{em} = 436, 462, 492 nm, corresponding to a bathochromic shift of about 2100–2200 cm^{-1} when compared to **9b**.

Nevertheless, for all the derivatives, the emission profile is relatively narrow and structured with a clear vibronic progression featuring a main vibrational mode in the order of 1250–1450 cm^{-1} mainly attributable to the C=C and C=N intramolecular vibrations. This is in nice agreement with the computational investigation as described in more detail below. Photoluminescence quantum yield (PLQY) values were in the order of 0.23–0.42 with the highest values recorded for compound **8b**. It is worth to notice that these values are much higher than those reported for parental, structurally related neutral 2,5-*bis*(4-pyridyl)-thiazolo[5,4-*d*]thiazole and 2,5-diphenyl-thiazolo[5,4-*d*]thiazole reported elsewhere,[24,25] in spite of the presence of the flexible (long) alkyl chains.

Time-resolved emission decay helped to shed a better light onto the kinetics and the nature of the emitting excited states. For all the compounds, the decay traces could be nicely fitted with a mono-exponential kinetic model that provides an emitting excited-state lifetime as short as 620, 432 and 496 ps for derivative **8b**, **9b** and **10b**, respectively. Hence, radiative (k_r) and non-radiative (k_{nr}) rate constants characterizing the emissive excited state could be estimated from lifetime and PLQY values by using the following equations (eqns. 1–2):

$$k_r = \text{PLQY} / \tau \qquad \text{(eqn. 1)}$$

$$k_{nr} = (1 - \text{PLQY}) / \tau \qquad \text{(eqn. 2)}$$

providing for all the derivatives similar k_r values in the order of 5.1–6.9 $x10^8$ s^{-1}, characteristic of a strongly allowed radiative process. Similarly, k_{nr} values are similar between the three series, being the values in the order of 0.9–1.7$x10^9$ s^{-1}, yet the lowest range values are observed for derivatives of series **8**, thus yielding the higher PLQY values within the different series. Overall, these data strongly support the rather similar nature of the excited state along the different compounds, with large $^1\pi$-π^* character mainly involving the common π-TzTz-π core, whereas the peripheral pyridines seem to be involved to a much lower extent for **9a** and **10b**. Instead, slightly larger involvement is expected for linear derivative **8b**, due to the longer π-conjugation

that also cover the peripheral pyridine moieties. This overall photophysical picture is also further corroborated by the little influence of the solvent polarity and the length of the alkyl chain on the efficiency of the radiationless deactivation channels (see Table 1 for compound **9b** as an example).

Going from fluid solution to thin-film in PMMA matrix at 20wt.% concentration of **8b**–**10b**, emission profiles become slightly broader and bathochromically shifted by about 20–25 nm. Concomitantly, PLQY decreases to 0.08, 0.12 and 0.10 for samples of compound **8b**, **9b** and **10b**, respectively. On the other hand, lifetime remains comparable and in the range of *ca.* 450 ps for *meta*-substituted derivatives **9b**–**10b**, but it becomes prolonged and characterized by a bi-exponential kinetics for derivative **8b**. The corresponding emission spectra and photophysical parameters can be found in Figure 2 and Table 2, respectively. These findings are indicative of the establishment of intermolecular π-π interactions between adjacent molecules in the solid state, a behavior that is much more pronounced for the linear **8b** compared to the two- and four-armed counterparts **9b**–**10b**.

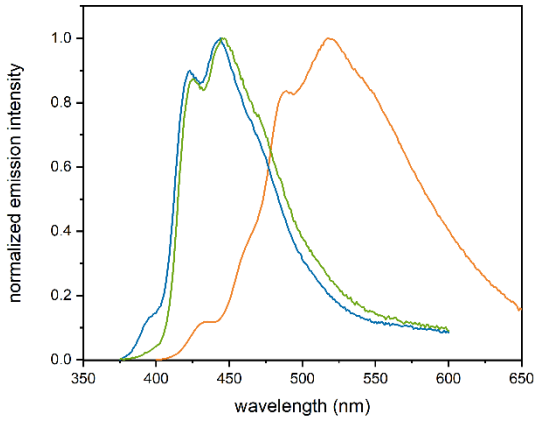

Figure 2. Normalized emission spectra of compound **8b** (orange), **9b** (blue), and **10b** (green) in PMMA thin film matrix at doping concentration of 20 wt.%. Emission spectra were recorded upon excitation at λ_{exc} = 360 nm for sample **8b** and **10b**; λ_{exc} = 320 nm for sample **9b**.

Previous investigations have shown that protonation of 2,5-diphenyl-TzTz in aqueous HCl quenches the emission of the TzTz core, resulting in a decrease of the PLQY from *ca.* 0.2 in organic solvents to a value below 0.05 in acidic conditions.[24] On the other hand, either protonation or alkylation of the pyridyl moieties of the 2,5-*bis*(pyridyl)-TzTz emitters gives rise to a dramatic enhancement of the PLQY reaching values up to 0.96.[25] Therefore, we wondered about the effect of protonation of the here investigated (**py**)$_n$-**π**-**TzTz**-**π**-(**py**)$_n$ systems, by investigating their optical properties in a solvent mixture composed of CH_2Cl_2 and trifluoroacetic acid (TFA) at 5% $^{V}/_{V}$. The corresponding spectra are shown in Figure 3 and the photophysical data are summarized in Table 3. In acidic media by TFA, electronic absorption spectra appear to be less intense, structureless and broader when compared to pure CH_2Cl_2 solvent. Surprisingly, a clear bathochromic shift of the absorbance was not observed upon protonation, with spectral onset and maxima being very similar in both conditions. In sharp contrast, all the three investigated compounds display a neat bathochromic shift in their emission spectrum that moves to 513 nm (–3440 cm^{-1}), 458 nm (–3239 cm^{-1}) and 434 nm (–1710 cm^{-1}), for derivative **8b**, **9b** and **10b** in their protonated form, respectively. This shift is accompanied by broadening and loss of the vibronic progression in the spectral profile, indicative of an increased ICT nature of the emitting excited state for the protonated forms compared to the neutral parental forms. Interestingly, while protonated **9b**–**10b** display a decrease of the PLQY down to 0.12 and 0.17 – values that are about half of those in pure CH_2Cl_2 –, protonation of **8b** give rises to an enhancement of PLQY that reaches a value as high as 0.52. For all the compounds, excitation spectra recorded at different emission wavelengths appear to be very similar and trace out the corresponding absorption spectrum. On the other hand, excited state emission decays become biexponential in nature. These findings point towards a possible dual-emission at the origin of the two distinct lifetimes, most likely due to an excited-state

tautomerism process (e.g. excited-state intramolecular proton transfer),[17] rather than two different ground state (protonated) forms.

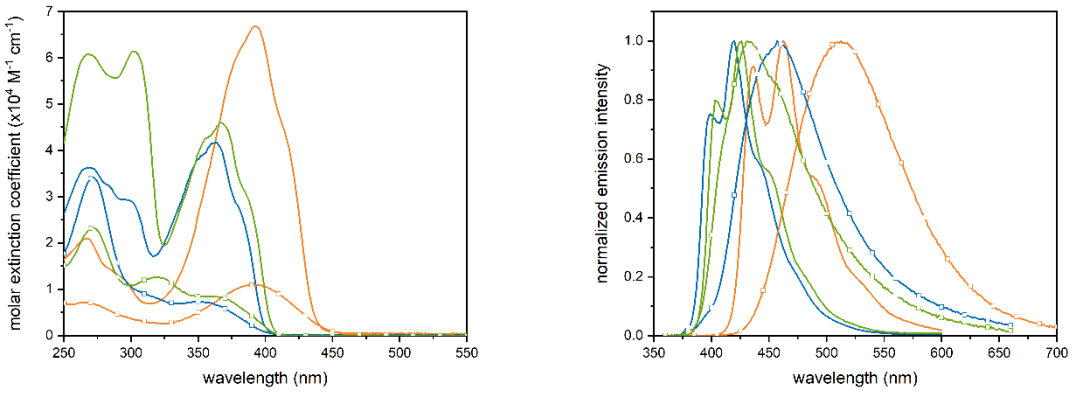

Figure 3. Electronic absorption (left box) and normalized emission (right box) spectra of compound **8b** (orange), **9b** (blue), and **10b** (green) in CH_2Cl_2 (solid traces) and in CH_2Cl_2:TFA 5% (solid traces + empty squares) at a concentration of 5×10^{-6} M at room temperature. Emission spectra were recorded upon excitation at λ_{exc} = 340–360 nm.

Table 1. Photophysical data of compound **8**–**10** in dilute (concentration 5×10^{-6} M) air-equilibrated CH_2Cl_2 solution at room temperature.

cmpd	medium	$\lambda_{max,abs}$ [nm] (ε [10^4 M^{-1} cm^{-1}])	λ_{em} [nm]	lifetime [ps]	PLQY[a]	k_r [10^8 s^{-1}]	k_{nr} [10^9 s^{-1}]	$E_{0,0}$ [eV][b]	Stokes shift [cm^{-1}][c]
8b	CH_2Cl_2	392 (6.68), 267 (2.09)	436, 462, 492, 530	620	0.42	6.84	0.93	2.92	2570
8c	CH_2Cl_2	393 (6.62), 265 (2.05)	437, 463, 492, 532	610	0.39	6.46	0.99	2.92	2560
9a	CH_2Cl_2	362 (3.37), 298 (2.17), 268 (2.82)	398, 419, 443	443	0.23	5.07	1.75	3.20	2500
9b	CH_2Cl_2	364 (4.17), 300 (2.90), 270 (3.62)	399, 419, 442	432	0.28	6.48	1.67	3.20	2410
9b	CH_3CN	360 (0.95), 271 (0.96), 231 (1.91)	397, 415, 437	440	0.35	7.85	1.49	3.25	2590
9b	DMF	364 (4.17), 300 (3.08)	397, 415, 437	454	0.29	6.28	1.57	3.18	2280
9c	CH_2Cl_2	363 (3.81), 300 (2.86), 269 (3.46)	399, 419, 442	443	0.28	6.34	1.62	3.20	2490
10a	CH_2Cl_2	368 (3.71), 301 (4.63), 266 (4.87)	404, 425, 450	499	0.27	5.53	1.49	3.15	2420
10b	CH_2Cl_2	367 (4.60), 302 (6.15), 269 (6.07)	404, 425, 451	496	0.34	6.76	1.34	3.15	2500
10c	CH_2Cl_2	367 (4.17), 302 (5.96), 2.69 (5.99)	404, 425, 451	511	0.33	6.37	1.32	3.15	2500

[a] Estimated by using quinine sulfate solution in aqueous H_2SO_4 0.5 M (PLQY reference value = 0.55); [b] $E_{0,0}$ is an estimated optical bandgap determined as the crossing point between the absorption and emission spectra; [c] Stokes' shift has been estimated as the difference between the maximum of the lowest-energy absorption band and the highest-energy emission peak.

Table 2. Photophysical data of compound **8b**, **9b** and **10b** in PMMA thin film at doping concentration of 20 wt.%.

cmpd	λ_{em} [nm]	lifetime [ps]	PLQY	k_r [10^8 s^{-1}]	k_{nr} [10^9 s^{-1}]
8b	461, 487, 518	1052 (46%) 278 (54%)	0.08	-	-
9b	422, 443	445	0.12	2.70	1.98
10b	424, 445	454	0.10	2.20	1.98

Table 3. Photophysical data of compound **8b**, **9b** and **10b** in dilute (concentration = 5×10^{-6} M) air-equilibrated CH_2Cl_2:TFA (5%) at room temperature.

cmpd	$\lambda_{max,abs}$ [nm] (ε [10^4 M^{-1} cm^{-1}])	λ_{em} [nm]	lifetime [ps]	PLQY
8b	393 (1.09), 269 (0.72)	513	602 (71%) 196 (29%)	0.52
9b	357 (0.71), 272 (3.42)	458	222 (59%) 722 (32%) 283 (9%)	0.12
10b	368 (0.82), 321 (1.26), 272 (2.33)	434	482 (30%) 1540 (70%)	0.17

Computational investigation

To support the interpretation of the photophysical data, the electronic structures of species **8**, **9** and **10** and their absorption and emission spectra were computed employing density functional and time-dependent density functional theory. Molecular orbital plots and energies, tables of calculated electronic transition properties and electron density-difference maps are displayed in Figure 4–7 and Table 4. For sake of computational time, alkyl chains were truncated at the methyl level, which correspond to computed species **8a**, **9a** and **10a**. Similar results are expected to be found for derivatives containing longer alkyl chains, such as **8b**–**10b** and **8c**–**10c**. Taking into account the rotation around bonds connecting the constituting rings and also the conformation assumed by the methoxy substituents, it is possible to foresee the existence of many different isomers for molecules **8a**–**10a**. However, only results obtained for the more stable conformer of each species are discussed in the following.

The 2,5-diphenylthiazolothiazole core of all the optimized species is invariably found to be almost exactly planar, in agreement with the geometry experimentally observed in the crystal structure of the corresponding unsubstituted molecule.[32] On the contrary, steric interactions involving the *ortho*-hydrogen atoms prevent the pyridyl substituents from lying in the same plane of the PhTzTzPh moiety. The dihedral angle between the planes defined by the pyridyl and the phenyl rings is quite similar in the three species (16.9, 17.2 and 15.8–17.9° for **8a**, **9a** and **10a**, respectively).

According to the calculations, the frontier molecular orbitals of **8a**–**10a** are mainly located on the diphenylthiazolothiazole core and can be related to the aromatic (HOMO) and the quinoid (LUMO) structure for this moiety (see Figure 4). In **9a**, the introduction of a 2-pyridyl substituent in *meta* on the phenyl rings allows to delocalize the FMOs only to a limited extent (14 and 2% for HOMO and LUMO, respectively). Adding a second substituent in *meta*, as in **10a**, does not significantly improve the delocalization over the pyridyl groups (15 and 5% for HOMO and LUMO, respectively). On the contrary, in **8a** the presence of a 2-pyridyl substituent

in *para* leads to a more substantial delocalization of the FMOs (28 and 13% for HOMO and LUMO, respectively). As a consequence, the destabilization of HOMO, the stabilization of LUMO and the corresponding reduction of the HOMO-LUMO energy gap with respect to the parent unsubstituted molecule is limited (and quite similar) for the two *meta*-substituted species **9a** and **10a** and is more pronounced for the *para*-substituted species **8a** (see Table 4).

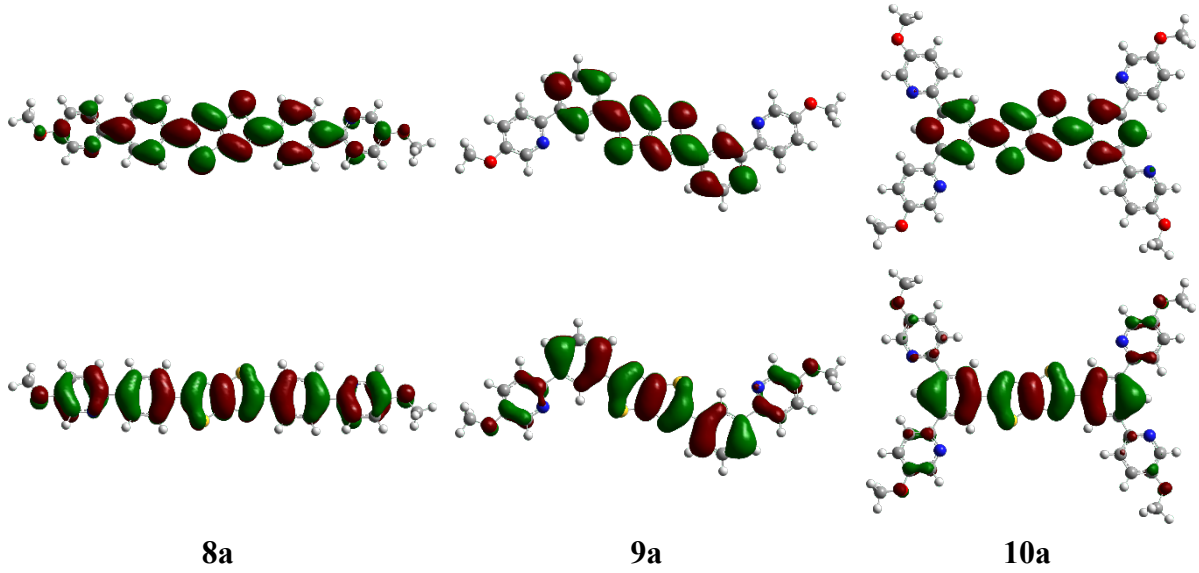

Figure 4. Isodensity surface plots for the HOMO (lower row) and LUMO (upper row) of **8a**, **9a** and **10a**.

Table 4. Computed HOMO and LUMO energy and energy gap for the unsubstituted PhTzTzPh and for **8a**, **9a** and **10a**.

	E_{HOMO} [eV]	E_{LUMO} [eV]	E_g [eV]
PhTzTzPh	–6.042	–2.027	4.015
8a	–5.720	–2.204	3.515
9a	–5.964	–2.035	3.930
10a	–5.942	–2.047	3.895

The absorption spectrum of these species is dominated by a broad $S_0 \rightarrow S_1$ HOMO-LUMO excitation at low energy, computed at 425, 373 and 378 nm for **8a**, **9a** and **10a**, respectively.

Figure 5 contains the corresponding electron density-difference maps for the three species, showing how the transition is essentially confined to the PhTzTzPh moiety for **9a** and **10a** while it encompasses also the pyridyl substituents for **8a**, albeit to a limited extent. As previously reported for similar species,[11,24] the presence of many different rotamers can explain the broadening observed for the absorption peak. Indeed, preliminary computations on the species **10a** allowed to identify at least ten stable conformers within 4 kJ from the global minimum, all significantly populated at room temperature, showing slight variations in the $S_0 \rightarrow S_1$ transition energy.

For the *para*-substituted species **8a**, similarly to the unsubstituted compound PhTzTzPh, the oscillator strength computed for the HOMO-LUMO excitation is much larger than those of any other below 250 nm. On the contrary, for the *meta*-substituted species **9a** and **10a**, other transitions at higher energy, not mainly centred on the TzTz core, contribute to the absorption spectra. In particular, for **9a** the $S_0 \rightarrow S_7$ excitation at 273 nm corresponds to a net charge transfer from the methoxopyridyl substituents to the phenyl rings. A similar transition ($S_0 \rightarrow S_9$), involving all the four methoxopyridyl substituents, can be found at 284 nm for **10a**, together with a transition ($S_0 \rightarrow S_{13}$) at 272 nm, corresponding to a net charge transfer from the methoxopyridyl substituents and the thiazolothiazole core to the phenyl rings. All these transitions are depicted by their corresponding electron density-difference maps in Figure 6.

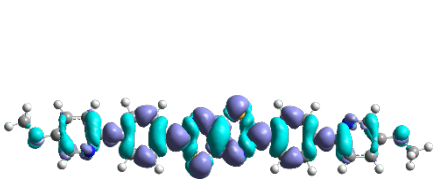

ΔE = 2.921 eV; λ = 425 nm
f = 2.3648
8a

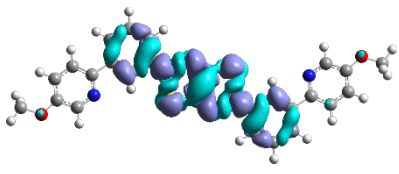

ΔE = 3.323 eV; λ = 373 nm
f = 1.4031
9a

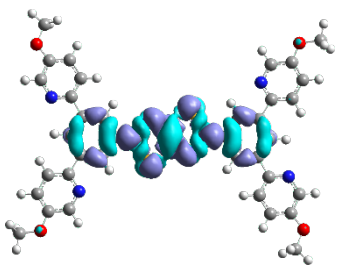

ΔE = 3.278 eV; λ = 378 nm
f = 1.5306
10a

Figure 5. Electronic density-difference maps for the $S_0 \rightarrow S_1$ HOMO-LUMO excitation of **8a**, **9a** and **10a**. Cyan and violet indicates a decrease and increase in electron density, respectively.

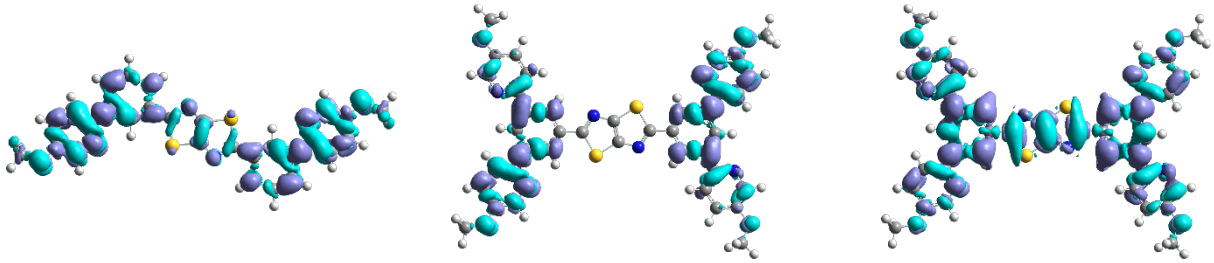

$S_0 \rightarrow S_7$
ΔE = 4.540 eV; λ = 273 nm
f = 0.9201
9a

$S_0 \rightarrow S_9$
ΔE = 4.366 eV; λ = 284 nm
f = 0.4874
10a

$S_0 \rightarrow S_{13}$
ΔE = 4.562 eV; λ = 272 nm
f = 0.6849
10a

Figure 6. Electronic density-difference maps for some of the more intense electronic transitions computed for **9a** and **10a**. Cyan and violet indicates a decrease and increase in electron density, respectively.

The optimized geometry of the lowest-lying singlet excited state for the three species shows the typical altered alternation of short and long bond lengths within the molecule, in agreement with the enhanced quinoid character of the excited state. The same conclusion can be formulated by looking at the electron density-difference maps for the emission $S_1 \rightarrow S_0$, whose features are almost superimposable to those describing the absorption. Both vertical and adiabatic energies have been computed for the $S_1 \rightarrow S_0$ transition. As expected, due to the substantial difference between the lowest-lying singlet excited state and the ground-state geometry, vertical and adiabatic values are quite different (ca. 0.26 eV). Although these computed values reproduce the observed trend, they underestimate the experimental values, especially in the case of the para-substituted species **8a** (see Figure 7). The vibrationally resolved emission spectra computed within the framework of the Franck-Condon principle reproduces reasonably well the observed additional maxima (464 and 491 nm *vs* 462 and 492 nm for **8a**, 423 and 449 nm *vs* 419 and 442 nm for **9a**, 428 and 456 nm *vs* 425 and 451 nm for **10a**). As expected for a thiazolothiazole-centered transition, the normal mode primarily

contributing to the vibronic structure of the band is the stretching of the central C–C bond of the condensed heterocycle (ν_{122} at 1483 cm^{-1}, ν_{124} at 1487 and ν_{180} at 1487 for **8a**, **9a** and **10a**, respectively).

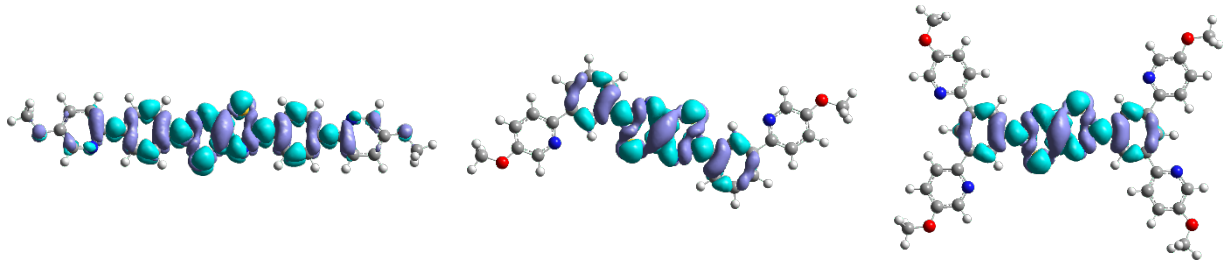

ΔE = 2.301 (*2.556*) eV	ΔE = 2.674 (*2.947*) eV	ΔE = 2.653 (*2.922*) eV
λ = 539 (*485*) nm	λ = 464 (*421*) nm	λ = 467 (*424*) nm
8a	**9a**	**10a**

Figure 7. Electronic density-difference maps computed (at the optimized S_1 geometry) for the vertical transition $S_1 \rightarrow S_0$ of **8a**, **9a** and **10a**. Energy computed for the corresponding adiabatic transition is also reported (*in italics*). Cyan and violet colour indicates a decrease and increase in electron density, respectively.

Conclusion

In conclusion, the synthesis of a novel family of thiazolo[5,4-*d*]thiazole fluorophores with general formula (**py**)$_n$-**π**-**TzTz**-**π**-(**py**)$_n$ (n = 1 or 2) is presented. The compounds bear peripheral alkoxy-pyridine moieties linked onto the central **-π-TzTz-π-** core at either the *para*- or *meta*-positions giving rise to either linear (compounds **8**), two- (compounds **9**) or four-armed (compounds **10**) molecular architectures. In CH_2Cl_2 solution, while the former display bluish-green emission with higher PLQY, the two latter possess near-UV to blue emission with somehow lower efficiency. In-depth steady-state and time-resolved photophysical investigation, along with TD-DFT computations, helped to assign the emission as π-π* in nature and involving the central **-π-TzTz-π-** for derivatives **9**–**10**, although it partially extends over the peripheral pyridine moieties for linear compounds **8**. Upon addition of an excess of TFA, emission spectra bathochromically shift as a consequence of the protonation of the

molecular emitters. Remarkably, different effects in the variation of PLQY were observed, with an enhancement of its value for series **8**, reaching a value as high as 0.52. The presented results widen the palette of a highly interesting, yet largely overlooked, class of small molecule emitters based on the TzTz scaffold and disclose the different effect exerted by the isomerism linkage of peripheral pyridines onto the emission properties in both non-protonated and protonated forms. Overall, these data will help to design more efficient molecular emitter based on the TzTz core in view of their potential applications as bio- and chemo-sensors as well as active materials in organic electronics.

Experimental Section

General considerations. All reagents were used as received without further purification unless differently stated. Silica gel for column chromatography was purchased from Sigma-Aldrich. ^{1}H and ^{13}C NMR spectra were recorded at 298 K on either Bruker AV300, Bruker AV400 or Bruker AV500 spectrometers in deuterated solvents and the residual solvent peak was used as the internal reference. ^{1}H and $^{13}C\{^{1}H\}$ NMR spectra were calibrated to residual solvent signals. All the chemical shifts (δ) are reported in ppm. High-resolution electrospray mass spectrometry (HR-ESI-MS) was performed by the Service Spectrométrie de Masse of the Fédération de Chimie "Le Bel" FR2010 of the University of Strasbourg. Experimental details on synthesis are available in the Supporting Information.

Photophysical characterization

Instrument details. Absorption spectra were measured on a Varian Cary 100 double-beam UV–VIS spectrophotometer and baseline corrected. Steady-state emission spectra were recorded on a Horiba Jobin−Yvon IBH FL-322 Fluorolog 3 spectrometer equipped with a 450 W xenon arc lamp, double-grating excitation, and emission monochromators (2.1 nm mm^{-1} of dispersion;

1200 grooves mm^{-1}) and a Hamamatsu R13456 red sensitive Peltier-cooled PMT detector. Emission and excitation spectra were corrected for source intensity (lamp and grating) and emission spectral response (detector and grating) by standard correction curves. Time-resolved measurements were performed using either the time-correlated single-photon counting (TCSPC) or the Multi-Channel Scaling (MCS) electronics option of the TimeHarp 260 board installed on a PicoQuant FluoTime 300 fluorimeter (PicoQuant GmbH, Germany), equipped with a PDL 820 laser pulse driver. A pulsed laser diode LDH-P-C-375 (λ = 375 nm, pulse full width at half maximum FWHM <50 ps, repetition rate 200 kHz–40 MHz) was used to excite the sample and mounted directly on the sample chamber at 90°. The photons were collected by a PMA Hybrid-07 single photon counting detector. The data were acquired by using the commercially available software EasyTau II (PicoQuant GmbH, Germany), while data analysis was performed using the built-in software FluoFit (PicoQuant GmbH, Germany). All the solvents were spectrophotometric grade.

Methods. For time resolved measurements, data fitting was performed by employing the maximum likelihood estimation (MLE) method. The quality of the fit was assessed by inspection of the reduced χ^2 function and of the weighted residuals. For multi-exponential decays, the intensity, namely *I*(t), has been assumed to decay as the sum of individual single exponential decays (Eqn. 3):

$$I(t) = \sum_{i=1}^{n} \alpha_i exp\left(-\frac{t}{\tau_i}\right) \qquad Eqn. 3$$

where τ_i are the decay times and α_i are the amplitude of the component at $t = 0$. In the tables, the percentages to the pre-exponential factors, α_i, are listed upon normalization.

Luminescence quantum yields were measured in optically dilute solutions (optical density <0.1 at the excitation wavelength) and compared to reference emitter by following the method of Demas and Crosby.[33,34] Quinine sulphate in 0.5 M H_2SO_4 (PLQY = 0.55)[35] was used as

reference fluorescence standard for samples. For thin-film and solution samples in CH_2Cl_2:TFA 95:5, the absolute PLQY were measured on a Hamamatsu Quantaurus-QY C11347-11 integrating sphere in air-equilibrated condition using an empty quartz tube as the reference upon excitation at λ_{exc} = 300–350 nm.

Computational details. Ground state and lowest-lying singlet excited state geometries were optimized by means of density functional and time-dependent density functional calculations. The parameter-free hybrid functional PBE0 [36] was employed along with the standard valence double-ζ polarized basis set 6-31G(d,p) for C, H, N, O and S. All the calculations were done in the presence of solvent (dichloromethane, used in the photophysical characterizations) described by a polarizable continuum model (PCM).[37] The nature of all the stationary points was checked by computing vibrational frequencies and all the geometries were found to be true minima. A preliminary conformational analysis was performed, taking into account the rotation around all the bonds linking the rings and the rotation of the methoxo substituents on the 2-pyridyl groups. For all the three species the global minimum possesses an exact C_i point symmetry. In order to simulate the absorption electronic spectrum down to about 250 nm the lowest 15 (or 25) singlet excitation energies were computed for **9a** and **10a** (or **8a**) by means of time-dependent density functional calculations. The vibrationally-resolved emission spectra were simulated in the framework of the Franck-Condon principle [38], shifting the 0–0 energy to its observed value. All the calculations were done with Gaussian 16.[39]

Acknowledgments

M.M. gratefully acknowledges the Université de Strasbourg, the CNRS, the International Centre for Frontier Research in Chemistry (icFRC), and the Labex CSC (ANR-10-LABX-0026 CSC) within the Investissement d'Avenir program ANR-10-IDEX-0002-02, the French Agence Nationale de Recherche (ANR) grant ANR-18-CE06-007-01 for financial support.

Supporting Information availability statement

Detailed synthetic procedures, supplementary ^{1}H and ^{13}C NMR spectra, and photophysical data can be found in the Supporting Information.

References

[1] Wong, M. Y.; Zysman-Colman, E. Purely Organic Thermally Activated Delayed Fluorescence Materials for Organic Light-Emitting Diodes. *Adv. Mater.* **2017**, *29*, 1605444. https://doi.org/10.1002/adma.201605444.

[2] Hong, G.; Gan, X.; Leonhardt, C.; Zhang, Z.; Seibert, J.; Busch, J. M.; Bräse, S. A Brief History of OLEDs—Emitter Development and Industry Milestones. *Adv. Mater.* **2021**, *33*, 2005630. https://doi.org/10.1002/adma.202005630.

[3] Chaudhry, M. U.; Muhieddine, K.; Wawrzinek, R.; Sobus, J.; Tandy, K.; Lo, S.; Namdas, E. B. Organic Light-Emitting Transistors: Advances and Perspectives. *Adv. Funct. Mater.* **2020**, *30*, 1905282. https://doi.org/10.1002/adfm.201905282.

[4] Mishra, A.; Fischer, M. K. R.; Bäuerle, P. Metal-Free Organic Dyes for Dye-Sensitized Solar Cells: From Structure: Property Relationships to Design Rules. *Angew. Chem. Int. Ed.* **2009**, *48*, 2474. https://doi.org/10.1002/anie.200804709.

[5] Wong, M. Y.; Zysman-Colman, E.; Adv. Mater., 2017, 29, 1605444. https://doi.org/10.1002/adma.201605444m.

[6] Takimiya, K.; Osaka, I.; Mori, T.; Nakano, M. Organic Semiconductors Based on [1]Benzothieno[3,2-b][1]Benzothiophene Substructure. *Acc. Chem. Res.* **2014**, *47*, 1493–1502. https://doi.org/10.1021/ar400282g.

[7] Perepichka, I. F. *Handbook of Thiophene-Based Materials*; John Wiley & Sons: Chichester, 2009.

[8] Rasmussen, S. C.; Evenson, S. J.; McCausland, C. B. Fluorescent Thiophene-Based Materials and Their Outlook for Emissive Applications. *Chem. Commun.* **2015**, *51*, 4528–4543. https://doi.org/10.1039/c4cc09206f.

[9] Kato, S.; Matsumoto, T.; Ishi-i, T.; Thiemann, T.; Shigeiwa, M.; Gorohmaru, H.; Maeda, S.; Yamashita, Y.; Mataka, S. Strongly Red-Fluorescent Novel Donor–π-Bridge–Acceptor–π-Bridge–Donor (D–π–A–π–D) Type 2,1,3-Benzothiadiazoles with Enhanced Two-

Photon Absorption Cross-Sections. *Chem. Commun.* **2004**, 2342–2343. https://doi.org/10.1039/b410016f.

[10] Borissov, A.; Maurya, Y. K.; Moshniaha, L.; Wong, W.-S.; Żyła-Karwowska, M.; Stępień, M. Recent Advances in Heterocyclic Nanographenes and Other Polycyclic Heteroaromatic Compounds. *Chem. Rev.* **2022**, *122*, 565–788. https://doi.org/10.1021/acs.chemrev.1c00449.

[11] Bevk, D.; Marin, L.; Lutsen, L.; Vanderzande, D.; Maes, W. Thiazolo[5,4-d]Thiazoles – Promising Building Blocks in the Synthesis of Semiconductors for Plastic Electronics. *RSC Adv.* **2013**, *3*, 11418. https://doi.org/10.1039/c3ra40851e.

[12] Dessì, A.; Calamante, M.; Mordini, A.; Zani, L.; Taddei, M.; Reginato, G. Microwave-Activated Synthesis of Thiazolo[5,4-d]Thiazoles by a Condensation/Oxidation Sequence. *RSC Adv.* **2014**, *4*, 1322–1328. https://doi.org/10.1039/c3ra45015e.

[13] Zahradník, P.; Magdolen, P.; Zahradník, P. Thiazolo[4,5-d]Thiazole—a New Domain for Potential Optoelectronic Application. *Tetrahedron Letters* **2010**, *51*, 5819–5821. https://doi.org/10.1016/j.tetlet.2010.08.110.

[14] Feng, Y.; Qiao, X.; Ouyang, G.; Liu, G.; Li, H. Thiazolothiazole-Based Quinoidal Compounds for High-Performance N-Channel Organic Field-Effect Transistors with Low-Cost Metal Electrodes. *Adv. Electron. Mater.* **2020**, *6*, 1901443. https://doi.org/10.1002/aelm.201901443.

[15] Ando, S.; Nishida, J.; Tada, H.; Inoue, Y.; Tokito, S.; Yamashita, Y. High Performance N-Type Organic Field-Effect Transistors Based on π-Electronic Systems with Trifluoromethylphenyl Groups. *J. Am. Chem. Soc.* **2005**, *127*, 5336–5337. https://doi.org/10.1021/ja042219.

[16] Dessì, A.; Calamante, M.; Sinicropi, A.; Parisi, M. L.; Vesce, L.; Mariani, P.; Taheri, B.; Ciocca, M.; Di Carlo, A.; Zani, L. Thiazolo[5,4-d]Thiazole-Based Organic Sensitizers with Improved Spectral Properties for Application in Greenhouse-Integrated Dye-Sensitized Solar Cells. *Sustainable Energy Fuels* **2020**, *4*, 2309–2321. https://doi.org/10.1039/d0se00124d.

[17] Zhang, Z.; Chen, Y.-A.; Hung, W.-Y.; Tang, W.-F.; Hsu, Y.-H.; Chen, C.-L.; Meng, F.-Y.; Chou, P.-T. Control of the Reversibility of Excited-State Intramolecular Proton Transfer (ESIPT) Reaction: Host-Polarity Tuning White Organic Light Emitting Diode on a New Thiazolo[5,4-d]Thiazole ESIPT System. *Chem. Mater.* **2016**, *28*, 8815–8824. https://doi.org/10.1021/acs.chemmater.6b04707.

[18] Subramaniyan, S.; Xin, H.; Kim, F. S.; Shoaee, S.; Durrant, J. R.; Jenekhe, S. A. Effects of Side Chains on Thiazolothiazole-Based Copolymer Semiconductors for High Performance Solar Cells. *Adv. Energy Mater.* **2011**, *1*, 854–860. https://doi.org/10.1002/aenm.201100215.

[19] Wang, K.; Zhang, H.; Chen, S.; Yang, G.; Zhang, J.; Tian, W.; Su, Z.; Wang, Y. Organic Polymorphs: One-Compound-Based Crystals with Molecular-Conformation- and Packing-Dependent Luminescent Properties. *Adv. Mater.* **2014**, *26*, 6168–6173. https://doi.org/10.1002/adma.201401114.

[20] Wang, K.; Huang, S.; Zhang, Y.; Zhao, S.; Zhang, H.; Wang, Y. Multicolor Fluorescence and Electroluminescence of an ICT-Type Organic Solid Tuned by Modulating the Accepting Nature of the Central Core. *Chem. Sci.* **2013**, *4*, 3288. https://doi.org/10.1039/c3sc51091c.

[21] Sayresmith, N. A.; Saminathan, A.; Sailer, J. K.; Patberg, S. M.; Sandor, K.; Krishnan, Y.; Walter, M. G. Photostable Voltage-Sensitive Dyes Based on Simple, Solvatofluorochromic, Asymmetric Thiazolothiazoles. *J. Am. Chem. Soc.* **2019**, *141*, 18780–18790. https://doi.org/10.1021/jacs.9b08959.

[22] Zhang, X.; Choi, H.-A.; Lee, S.; Yin, J.; Kim, S. H.; Lee, C.; Yoon, J. A Cholesteryl Thiazolothiazole Derivative for Colorimetric Sensing of Cu^{2+} and Its Sol–Gel Transition. *Dyes and Pigments* **2015**, *122*, 109–115. https://doi.org/10.1016/j.dyepig.2015.06.016.

[23] Jung, J. Y.; Han, S. J.; Chun, J.; Lee, C.; Yoon, J. New Thiazolothiazole Derivatives as Fluorescent Chemosensors for Cr^{3+} and Al^{3+}. *Dyes and Pigments* **2012**, *94*, 423–426. https://doi.org/10.1016/j.dyepig.2012.02.005.

[24] Pinto, M. R.; Takahata, Y.; Atvars, T. D. Z. Photophysical Properties of 2,5-Diphenyl-Thiazolo[5,4- d]Thiazole. *J. Photochem. Photobiol. A: Chemistry* **2001**, *143*, 119–127. https://doi.org/10.1016/s1010-6030(01)00520-2.

[25] Woodward, A. N.; Kolesar, J. M.; Hall, S. R.; Saleh, N.-A.; Jones, D. S.; Walter, M. G. Thiazolothiazole Fluorophores Exhibiting Strong Fluorescence and Viologen-Like Reversible Electrochromism. *J. Am. Chem. Soc.* **2017**, *139*, 8467–8473. https://doi.org/10.1021/jacs.7b01005.

[26] Roy, I.; Bobbala, S.; Zhou, J.; Nguyen, M. T.; Nalluri, S. K. M.; Wu, Y.; Ferris, D. P.; Scott, E. A.; Wasielewski, M. R.; Stoddart, J. F. ExTzBox: A Glowing Cyclophane for Live-Cell Imaging. *J. Am. Chem. Soc.* **2018**, *140*, 7206–7212. https://doi.org/10.1021/jacs.8b03066.

[27] Zhou, J.; Wu, Y.; Roy, I.; Samanta, A.; Stoddart, J. F.; Young, R. M.; Wasielewski, M. R. Choosing Sides: Unusual Ultrafast Charge Transfer Pathways in an Asymmetric Electron-Accepting Cyclophane That Binds an Electron Donor. *Chem. Sci.* **2019**, *10*, 4282–4292. https://doi.org/10.1039/c8sc05514a.

[28] Tang, B.; Li, W.; Chang, Y.; Yuan, B.; Wu, Y.; Zhang, M.; Xu, J.; Li, J.; Zhang, X. A Supramolecular Radical Dimer: High-Efficiency NIR-II Photothermal Conversion and Therapy. *Angew. Chem. Int. Ed.* **2019**, *58*, 15526–15531. https://doi.org/10.1002/anie.201910257.

[29] Sasabe, H.; Chiba, T.; Su, S.-J.; Pu, Y.-J.; Nakayama, K.; Kido, J. 2-Phenylpyrimidine Skeleton-Based Electron-Transport Materials for Extremely Efficient Green Organic Light-Emitting Devices. *Chem. Commun.* **2008**, 5821. https://doi.org/10.1039/b812270a.

[30] Sasabe, H.; Gonmori, E.; Chiba, T.; Li, Y.-J.; Tanaka, D.; Su, S.-J.; Takeda, T.; Pu, Y.-J.; Nakayama, K.; Kido, J. Wide-Energy-Gap Electron-Transport Materials Containing 3,5-Dipyridylphenyl Moieties for an Ultra High Efficiency Blue Organic Light-Emitting Device. *Chem. Mater.* **2008**, *20*, 5951–5953. https://doi.org/10.1021/cm801727d.

[31] Su, S.-J.; Takahashi, Y.; Chiba, T.; Takeda, T.; Kido, J. Structure-Property Relationship of Pyridine-Containing Triphenyl Benzene Electron-Transport Materials for Highly Efficient Blue Phosphorescent OLEDs. *Adv. Funct. Mater.* **2009**, *19*, 1260–1267. https://doi.org/10.1002/adfm.200800809.

[32] Li, D.; Zhang, Z.; Zhao, S.; Wang, Y.; Zhang, H.; Diboron-containing fluorophores with extended ladder-type π-conjugated skeletons. *Dalton Trans* **2011**, 1279–1285. https://doi.org/10.1039/C0DT01269F.

[33] Crosby, G. A.; Demas, J. N. Quantum Efficiencies of Transition-Metal Complexes. I. d-d Luminescence. *J. Am. Chem. Soc.* **1970**, *92*, 7262–7270. https://doi.org/10.1021/ja00728a006.

[34] Ishida, H.; Bünzli, J.-C.; Beeby, A. Guidelines for Measurement of Luminescence Spectra and Quantum Yields of Inorganic and Organometallic Compounds in Solution and Solid State (IUPAC Technical Report). **2016**, *88*, 701–711. https://doi.org/10.1515/pac-2014-0706.

[35] Brouwer, A. M. Standards for Photoluminescence Quantum Yield Measurements in Solution (IUPAC Technical Report). **2011**, *83* (12), 2213–2228. https://doi.org/10.1351/pac-rep-10-09-31.

[36] Adamo, C.; Barone, V. Toward Reliable Density Functional Methods without Adjustable Parameters: The PBE0 Model. *J. Chem. Phys.* **1999**, *110*, 6158–6170. https://doi.org/10.1063/1.478522.

[37] Scalmani, G.; Frisch, M. J. Continuous Surface Charge Polarizable Continuum Models of Solvation. I. General Formalism. *J. Chem. Phys.* **2010**, *132*, 114110. https://doi.org/10.1063/1.3359469.

[38] Barone, V.; Bloino, J.; Biczysko, M.; Santoro, F. Fully Integrated Approach to Compute Vibrationally Resolved Optical Spectra: From Small Molecules to Macrosystems. *J. Chem. Theory Comput.* **2009**, *5*, 540–554. https://doi.org/10.1021/ct8004744.

[39] Gaussian 16 (revision A.03), Gaussian Inc., Wallingford, CT, **2016**.